Structural influence on the femtosecond laser ability to create fluorescent patterns in silver-containing sodium-gallium phosphate glasses

Théo Guérineau, Laura Loi, Yannick Petit, Sylvain Danto, Alexandre Fargues, Lionel Canioni, Thierry Cardinal

Research Article | Vol. 8, No. 12 | 1 Dec 2018 | OPTICAL MATERIALS EXPRESS 3748
Optical Materials EXPRESS

Structural influence on the femtosecond laser ability to create fluorescent patterns in silver-containing sodium-gallium phosphate glasses

THÉO GUÉRINEAU,[1,*] LAURA LOI,[2] YANNICK PETIT,[1,2] SYLVAIN DANTO,[1] ALEXANDRE FARGUES,[1] LIONEL CANIONI,[2] AND THIERRY CARDINAL[1]

[1]*Université de Bordeaux, CNRS, ICMCB, UPR 9048, F-33608 Pessac, France*
[2]*Université de Bordeaux, CNRS, CEA, CELIA, UMR 5107, F-33405 Talence, France*
**theo.guerineau@u-bordeaux.fr*

Abstract: Silver containing glasses in the P_2O_5 - Ga_2O_3 - Na_2O ternary diagram have been investigated to relate the effect of glass network structure and sodium ions concentration to spectroscopic and laser-writing properties of the materials. The first and most striking evidence is the large gain in the photosensitivity of fluorescent molecular silver clusters, and thus three-dimensional laser-induced patterns, from the meta-phosphate to the pyro-phosphate and ortho-phosphate glass compositions. This effect has been related to the progressive increase of the initial silver pairing quantity considering the shortening of the phosphate chains and the increase of the sodium ions concentration. One believes the presented detailed consideration of structure/property relationship will impact the design of new photosensitive glasses applied to the laser-manufacturing of components for photonic integrated circuits.

1. Introduction

In the last ten years femtosecond laser writing has become a versatile tool for engineering various optical microcomponents in transparent inorganic vitreous materials for applications in fields such as astrophotonics, optical communications, optofluidics or sensing [1–3]. Numerous investigations have been devoted to commercial materials, such as fused silica, highlighting material modifications such as refractive index changes and void creations [4,5].

In the meantime interest has grown in the development of specially-designed silver containing phosphate glasses [6–8]. The introduction of silver has appeared as the most efficient and fruitful route toward the functionalization of glasses with distinctive properties. Photo-written silver containing phosphate glasses are of particular interest since they offer the possibility to induce various linear or nonlinear photo-produced optical properties [9–15]. So far however, to the best of our knowledge, limited attention has been paid to the relation between the photosensitivity of the photo-induced silver clusters and the glass network.

Most common phosphate glasses are characterized by the length of the phosphate chains made of PO_4 tetrahedrons. The usual description of the glass phosphate network is based on Q^n units, where Q represents the PO_4 tetrahedron and n the number of bridging oxygen between phosphorus elements. In a meta-phosphate glass, the network is formed of infinite chains with Q^2 units, while pyro-phosphate are formed of Q^1 dimers and orthophosphate of isolated Q^0, respectively corresponding to O/P ratios of 3, 3.5, and 4 [16]. Here in the silver-containing P_2O_5 - Ga_2O_3 - Na_2O glass system we correlate the materials compositions and physico-chemical properties with the glass network structures, the photosensitivity property of the material under femtosecond laser irradiation, and more specifically with the conditions for the silver clusters generation.

#345384 https://doi.org/10.1364/OME.8.003748
Journal © 2018 Received 10 Sep 2018; revised 26 Oct 2018; accepted 30 Oct 2018; published 7 Nov 2018

Optical Materials EXPRESS

2. Experimental method

2.1. Glass preparation

A series of glasses has been elaborated in the ternary system P_2O_5 - Ga_2O_3 - Na_2O with a fixed amount of added silver to investigate the three phosphate networks meta-, pyro- and ortho-phosphate. The investigated series corresponds to the nominal composition in Mol% $98[(Na_2O)_x + (74P_2O_5 + 26Ga_2O_3)_{100-x}] + 2Ag_2O$ (hereafter GPN_x:Ag series) with x = 15, 26, 35, 42, 47 and 51 Mol%. Recent studies performed by associates [17] conducted on compositions of the same glass system show that the maximal discrepancy between nominal and experimental compositions is less than 3 Mol% for each precursor. The P_2O_5 – Ga_2O_3 – Na_2O ternary diagram and the GPN_x line are reported on Fig. 1.

The corresponding nominal compositions, with the O/P and Ga_2O_3/P_2O_5 ratios are described in Table 1. Glasses were synthetized from H_3PO_4 (Roth, 85%), Ga_2O_3 (Strem Chemicals, 99.998%), Na_2CO_3 (Alfa Aesar, 99.95%), and $AgNO_3$ (Alfa Aesar, 99.995%). All precursors were mixed together into a Teflon beaker in aqueous solution and gently dried on a sand bath for one night. The solid mixture was ground and then melt in a platinum crucible between 1050°C and 1200°C (depending on the composition) during 14 hours in order to obtain a homogenous repartition of Ag^+ silver ions. All samples were annealed 30°C below the glass transition T_g (386°C ≤ T_g ≤ 556°C) for 4 hours, cut (150 µm and 1 mm-thick) and optically polished on both parallel faces.

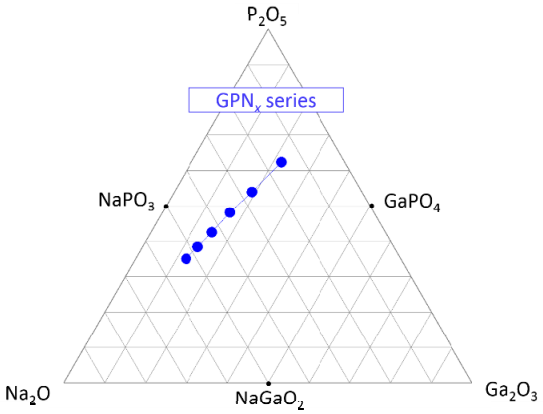

Fig. 1. Ternary diagram of P_2O_5 - Ga_2O_3 - Na_2O with investigated compositions (blue dots) (note all compositions contain 2 Mol% of silver oxide in addition, corresponding to the GPN_x:Ag series)

Table 1. Investigated glasses in the GPN_x:Ag series: acronym, sodium content x (Mol%), nominal compositions and ratios (O/P and Ga_2O_3/P_2O_5)

Acronym	x	P_2O_5	Ga_2O_3	**Na_2O**	Ag_2O	O/P	Ga_2O_3 / P_2O_5
GPN_{15}:Ag	15	61.14	21.58	**15.28**	2.00	3.2	0.35
GPN_{26}:Ag	26	52.89	18.67	**26.44**	2.00	3.3	0.35
GPN_{35}:Ag	35	46.60	16.45	**34.95**	2.00	3.4	0.35
GPN_{42}:Ag	42	41.65	14.70	**41.65**	2.00	3.6	0.35
GPN_{47}:Ag	47	37.65	13.29	**47.06**	2.00	3.7	0.35
GPN_{51}:Ag	51	34.35	12.12	**51.23**	2.00	3.8	0.35

Optical Materials EXPRESS

2.2. Glass analysis

The density, ρ, was determined by the Archimedes method using diethyl phthalate as an immersion liquid at room temperature with a Fisher scientific Sartorius YDK01. The measurement precision is estimated to be ± 0.01 g.cm^{-3}. Refractive indices were measured with an Abbe refractometer at 480, 589, 644 and 656 nm with an accuracy of ± 0.002.

Raman spectra were recorded in the range of 400 – 1400 cm^{-1} at room temperature with a resolution of 2.5 cm^{-1} using a LABRAM 800-HR Raman spectrometer (Horiba Jobin-Yvon) while excited with a single longitudinal mode laser source at 532 nm. Micro-Raman spectroscopy was collected with a microscope objective with 50 × – NA 0.75, ensuring a micron-scale spatial resolution.

The UV-visible transmission spectra were recorded on a Cary 5000 (Varian) spectrometer on 150 µm-thick samples from 200 nm to 800 nm by step of 1 nm.

The luminescence spectra (emission and excitation) were recorded with a SPEX Fluorolog-2 spectrofluorimeter (Horiba Jobin-Yvon) at room temperature on glass powder. The excitation source was a 450 W xenon lamp with a continuous excitation from 200 nm to 800 nm. Each spectrum was carried out with a step and resolution of 1 nm. A Hamamatsu R298 photomultiplier was used to detect and amplify the signal.

2.3. Femtosecond Direct Laser Writing (DLW)

DLW were performed on 1 mm-thick glass samples thanks to a KGW:Yb femtosecond oscillator (up to 2.6 W, 9.1 MHz, 390 fs FWHM at 1030 nm) combined with an acousto-optic modulator to control the number and the energy of pulses, thus enabling several irradiances from 1.8 to 16.4 TW.cm^{-2}. Spherical aberrations were mostly corrected by the use of a spatial light modulator (LCOS; X10468-03, Hamamatsu Photonics). A high-precision 3D translation stage XMS-50 (better than 50 nm resolution) was used to perform the sample positioning and displacements with various velocities from 25 µm.s^{-1} to 500 µm.s^{-1}. An Olympus microscope objective (20 × , NA 0.75) was used to produce the photo-induced structures, 160 µm below the sample surface.

2.4. DLW glass structuration analysis

Micro-luminescence was conducted with a LABRAM 800-HR spectrophotometer (Horiba Jobin-Yvon) and an Olympus microscope objective (50 × , NA 0.75) using an excitation laser diode at 405 nm (100 mW, TEM 00, OBIS, COHERENT) and thermoelectric cooled CCD Camera (Synapse Model 354308). The collected spectra were corrected for detection arm spectral response by the correction function determined using reference samples with broad spectral emission.

Wide-field fluorescence imaging was made thanks to a Leica DMI 3000 M inverted microscope using a Leica SFL 100 diode enabling an excitation at 365 nm and the fluorescence collection recorded with a Leica MC 120 HD camera. Microscope objectives N PLAN EPI 10 × , NA 0.25 and 50 × , NA 0.75 were used.

3. Results

3.1 Glass properties

Glass properties for GPN_x:Ag series have been measured. It includes density, Raman spectroscopy, refractive index dispersion and optical transmission (Fig. 2). The dependence of the density with x shows a slight increase from ρ = 3.03 g.cm^{-3} (x = 15) to ρ = 3.07 g.cm^{-3} (x = 35) (Fig. 2(a)). Then it decreases strongly, up to ρ = 2.94 g.cm^{-3} (x = 51).

The Raman spectroscopy is depicted on Fig. 2(b). It shows a continuous spectrum evolution with x. Corresponding Raman peak assignments and associated references are listed in Table 2. Between 15 and 35 Mol% Na_2O, the major band contributions are centered at 690

Optical Materials EXPRESS

cm^{-1} and 1150 cm^{-1}. They are assigned respectively to symmetric P-O-P bond stretching vibrations between two Q^2 on the one hand, and to (PO_2^-) symmetric stretching vibrations in Q^2 entities on the other hand. In the high-frequency range of the spectrum we observed an increase of the intensity of the band at 1200-1286 cm^{-1} with x which corresponds to asymmetric (PO_2^-) stretching vibrations in Q^2 phosphorus tetrahedra, and in the meantime, a decrease of the band at 1287-1330 cm^{-1} related to symmetric (P = O) stretching in Q^3 tetrahedra.

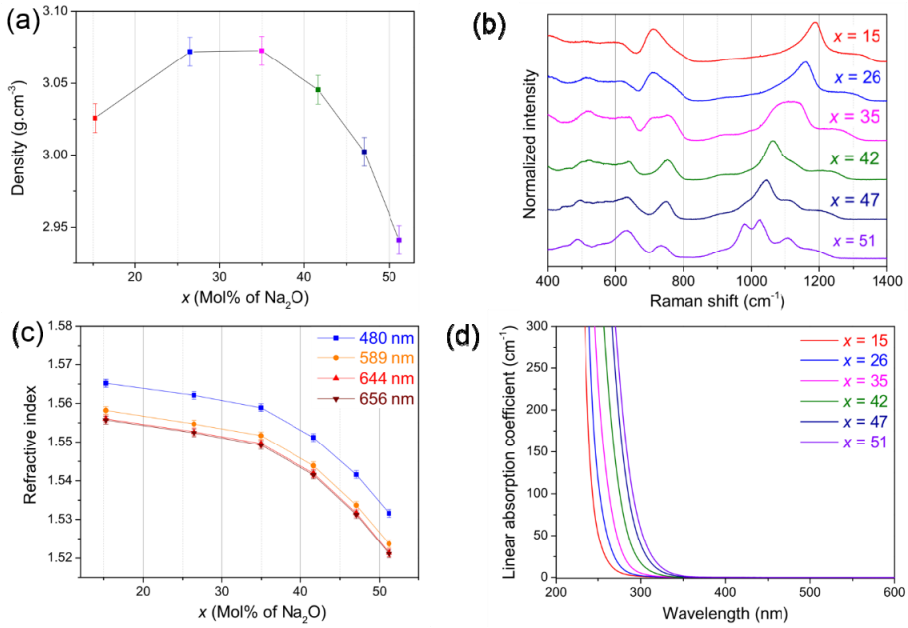

Fig. 2. Properties of the GPN_x:Ag series as function of the Na_2O content x (a) Density (b) Normalized raw Raman spectra (c) Refractive indices measured at 480, 589, 644 and 656 nm and (d) Linear absorption coefficient spectra in UV-visible region. Lines are guides for the eyes for (a) and (c).

When the Na_2O content reaches x = 35 and above, other major contributions appear and gradually increase. In fact, GaO_4 bending and stretching vibrations are respectively observed at 500 and 640 cm^{-1}. Additionally, symmetric and asymmetric P-O-P bond stretching in pyrophosphate entities, but also symmetric and asymmetric (PO_3^{2-}) stretching in Q^1, appear at 750, 920, 1000-1050 and 1100 cm^{-1} respectively. The symmetric (PO_4^{3-}) stretching of Q^0 at 980 cm^{-1} is merely visible at high sodium content (above 40 Mol% of Na_2O). The GPN_{35}:Ag has an intermediate Raman signature since it includes most of the Raman characteristics of all of the GPN_x:Ag glasses.

The linear refractive index evolution is shown in Fig. 2(c), the trend being similar for each measured wavelengths. It decreases slowly with x up to 35 Mol% of Na_2O and more sharply beyond. The linear absorption coefficient of the GPN_x:Ag series is depicted in Fig. 2(d). It is reported for values up to 300 cm^{-1} for 150 µm-thick samples. Between 250 nm and 350 nm, the absorption coefficient increases sharply due to the presence of the silver ions Ag^+ [18], such silver absorption edge showing a shift towards high energies when the sodium content decreases.

The luminescence properties of the GPN_x:Ag series are presented in Fig. 3. Figure 3(a) represents the typical excitation and emission luminescence of the GPN_{15}:Ag glass [28,29]. For an excitation at 220 nm (Fig. 3(a) - blue curve), one emission band is observed with two maximum contributions at 290 nm and 380 nm, corresponding to two distinct silver glassy

Optical Materials EXPRESS

types of environment respectively labeled A and B. For a fluorescence emission at 290 nm (Fig. 3(a) - black curve), the maximal excitation spectrum shows a maximum at 220 nm, which is attributed to the transition $d^{10} \rightarrow d^9s^1$ of isolated Ag^+ silver ion environments (sites A). Such silver ions are far enough from each other to do not presented any observable atomic orbital modifications with a spectrofluorimeter.

Table 2. Raman bands assignment in silver-doped gallo-phosphate glasses

Peak position	Raman bands assignment	Ref.
~350 cm^{-1}	GaO_6 vibration mode	[19]
~500 cm^{-1}	GaO_4 bending	[17,20]
~640 cm^{-1}	GaO_4 stretching vibrations	[17,19–23]
~690 cm^{-1}	P-O-P bonds symmetric stretching vibrations in Q^2	[17,19,24]
~750 cm^{-1}	P-O-P bonds symmetric stretching vibrations in Q^1	[17,19,21,24,25]
~920 cm^{-1}	Asymmetric P-O-P vibrations in Q^1	[17,19,21]
~980 cm^{-1}	Symmetric (PO_4^{3-}) stretching in Q^0 vibrations	[17,24]
~1000-1050 cm^{-1}	Symmetric vibrations of (PO_3^{2-}) Q^1 entities	[17,19,24,26]
~1100 cm^{-1}	Asymmetric (PO_3^{2-}) Q^1 vibrations	[17,19,26]
~1150 cm^{-1}	(PO_2^-) Q^2 symmetric stretch vibrations	[17,19,24,26]
~1200-1286 cm^{-1}	Asymmetric PO_2 stretch of Q^2	[17,19,24,26]
~1287-1330 cm^{-1}	(P = O) symmetric Q^3 stretching	[17,26,27]

For a fluorescence emission at 380 nm (Fig. 3(a) - red curve), the excitation spectrum displays a maximum at 250 nm, which is attributed to the presence of silver ions in close vicinity, such as the dimer Ag^+-Ag^+ observed in crystalline compounds (sites B) [30]. According to lifetime measurements (not shown here) no resonant transfer has been evidenced between the A and B emitter types. The emission spectra of the glasses for excitation at 220 nm are presented in Fig. 3(b). When the sodium content *x* increases from 15 to 51 Mol%, the overall emission drops, with a decrease of the B type emission while the A one vanishes. The spectral dependence with *x* is accompanied with a red spectral shift for both A and B emissions. Indeed, up to 26 Mol% of Na_2O, the A band decreases while the B one is not affected. Above 26 Mol% of Na_2O, the intensity of the site B starts to decline as well while remaining more intense than the emitter A. The normalized excitation spectra of the GPN_x:Ag glasses (x = 15, 26 and 51) for an emission at 380 nm are reported in Fig. 3(c). When x = 15, the maximum of the excitation band is below 250 nm. For x = 51 one can clearly distinguish a second band with a maximum peaking at around 270 nm. The situation is intermediate for the last spectrum corresponding to x = 26.

Optical Materials EXPRESS

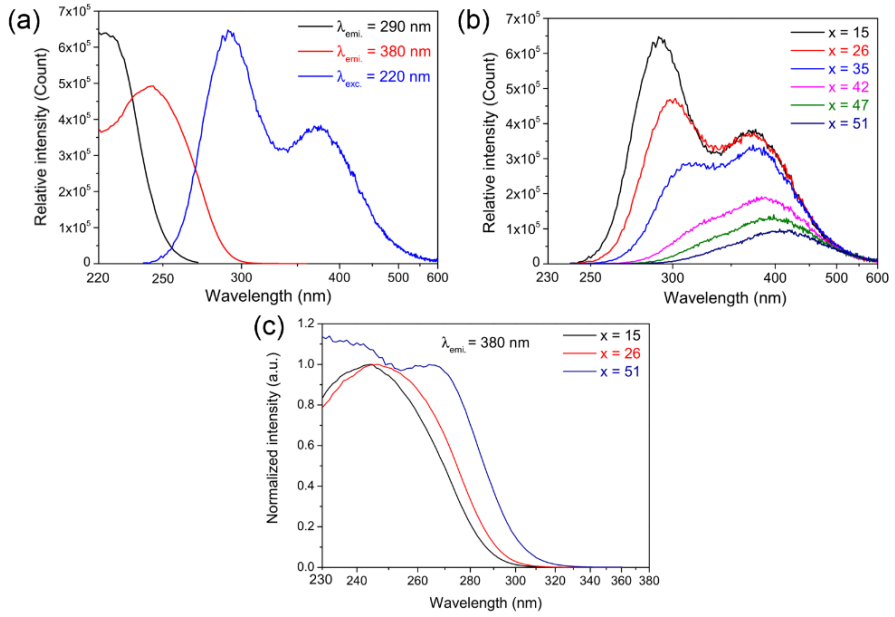

Fig. 3. (a) Excitation and emission spectra of GPN_{15}:*Ag* glass (b) Emission spectra of both isolated Ag^+ ions and Ag^+-Ag^+ dimers with a selective excitation of the isolated Ag^+ ions at 220 nm and (c) Selective excitation spectra of Ag^+-Ag^+ dimers for an emission at 380 nm in GPN_{15}:Ag series. The inset shows the normalized excitation spectra of Ag^+-Ag^+ dimers for an emission at 380 nm in GPN_x:Ag series.

3.2 Direct laser writing in GPN_x:Ag

The DLW was conducted on GPN_x:Ag glasses. All samples show the capacity to be laser inscribed, with parameters depending on their composition, as detailed hereafter. A laser-structuring "velocity-irradiance" matrix for various sample motion velocities and laser irradiances is presented in Fig. 4(a). It is displayed for the GPN_{26}:Ag glass, showing an image of the wide-field UV excitation of the fluorescence for an excitation at 365 nm.

No photo-induced luminescence is observed below an irradiance of 6.7 $TW.cm^{-2}$. This result is true for all glasses in the GPN_x:Ag series. Laser-induced fluorescent structures in the red square (solid line) were imaged with an exposure time 4.5 shorter than the ones in the green square (Fig. 4(a)). Careful precautions were taken to ensure that images showed no saturation. For a constant velocity, the fluorescence intensity increases with irradiance, whereas at constant irradiance, and starting from 9.5 $TW.cm^{-2}$, the fluorescence intensity decreases with sample velocity. Considering both irradiance and velocity, the highest fluorescence intensity for the GPN_{26}:Ag glass is obtained for an irradiance of 16.3 $TW.cm^{-2}$ and a sample motion of 25 $\mu m.s^{-1}$, while the less intense one corresponds to an irradiance of 6.7 $TW.cm^{-2}$ and a sample motion of 25 $\mu m.s^{-1}$. An entire photo-inscribed structure for the GPN_{26}:Ag glass, written at 9.5 $TW.cm^{-2}$ and 500 $\mu m.s^{-1}$, is shown in Fig. 4(b). Using the digital zoom, one can observe in Fig. 4(c) two parallel fluorescent lines. Such lines correspond to the top view of two parallel fluorescent planes. As previously reported [12,31], the interaction voxel is surrounded by permanent luminescent silver clusters Ag_m^{x+} while in the center the combination of both photo-dissociation and silver diffusion leads to the silver element depletion and the absence of fluorescent clusters. Indeed, both sample motions and laser parameters contribute to generate two parallel planes with depth and distance corresponding respectively to the confocal parameter and spot diameter, namely two-fluorescent-plane inscription regime. Such an induced silver element redistribution and silver cluster creation result from the many-pulses interaction, with in our specific case a pulse

Optical Materials EXPRESS

accumulation ranging from 4×10^4 pulses (velocity 500 µm.s^{-1}) to 7.4×10^5 pulses (velocity 25 µm.s^{-1}). At the lowest irradiance of 6.7 TW.cm^{-2} (Fig. 4(d)), the photo-structured square shows a weak luminescence. By digitally zooming, as shown in Fig. 4(e), one cannot observe the two-fluorescent-plane. This irradiation parameter leads here to the one-fluorescent-track inscription regime.

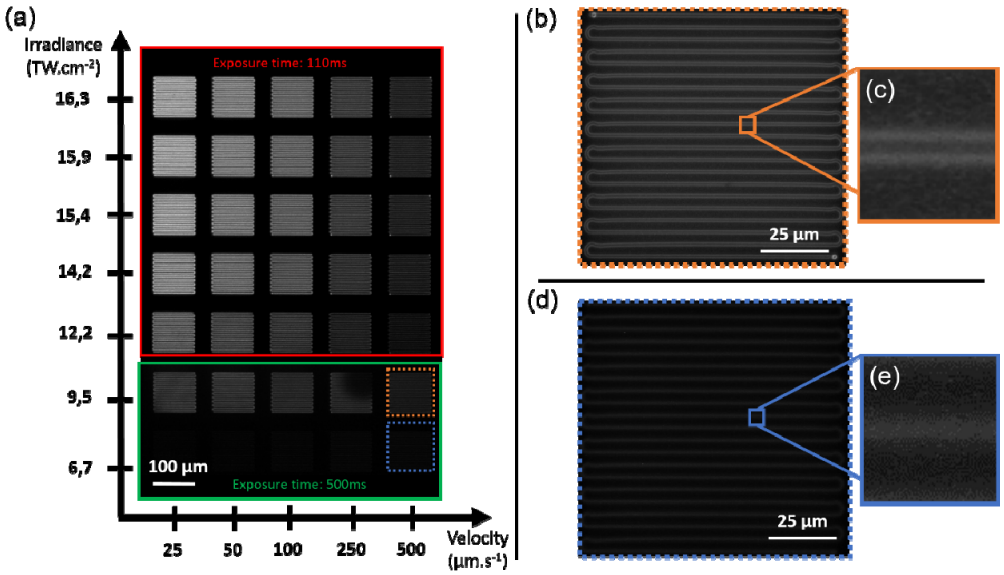

Fig. 4. Wide-field fluorescence imaging of the GPN_{26}:Ag glass with excitation at 365 nm (a) Fluorescent coil structures of 100x100 µm^2 for various DLW irradiances and velocities (b, d) Individual coil structures created 500 µm.s^{-1} and at 9.5 TW.cm^{-2} or 6.7 TW.cm^{-2}, respectively (c, e) Associated digital zooms.

The micro-luminescence spectrum analysis of all GPN_x:Ag glasses was performed. For the sake of clarity, only the GPN_{15}:Ag, GPN_{26}:Ag and GPN_{51}:Ag cases are presented here, corresponding respectively to meta-phosphate (O/P = 3.2), pyro-phosphate (O/P = 3.3) and ortho-phosphate glasses (O/P = 3.8). The respective luminescence emission spectra of the glasses for an excitation of 405 nm and a velocity of 25 µm.s^{-1} are shown in Fig. 5(a)-5(c).

The silver clusters emission spectrum in meta-phosphate (x = 15) obtained for 16.3 TW.cm^{-1} has a band shape covering the entire visible range, with a maximum at around 500 nm (Fig. 5(a) - black curve). This typical luminescence is attributed to the presence of Ag_m^{x+} silver clusters [32]. When decreasing in irradiance up to 9.5 TW.cm^{-2}, the spectrum distribution remains constant. At 6.7 TW.cm^{-2}, the maximum emission shifts at 650 nm and its intensity drops drastically (Fig. 5(a) - red curve). This red-shifted emission can be related to hole traps, namely the Ag^{2+} entities [33]. The pyro-phosphate glass for an irradiance of 16.3 TW.cm^{-2} presents a similar spectral distribution to the meta-phosphate one (Fig. 5(b) - black curve). The spectrum slightly shifts towards higher wavelengths when irradiance decreases at 9.5 TW.cm^{-2}, while its intensity drops by a factor of 22 (Fig. 5(b) - red curve). When decreasing the irradiance down to 6.7 TW.cm^{-2}, the fluorescence nearly vanishes, while its maximum fluorescence shifts again at 650 nm (Fig. 5(b) - blue curve). Concerning the ortho-phosphate sample, and regardless of the irradiance, the emission spectral distribution remains unchanged as shown in Fig. 5(c). The maximum intensity is centered on 450 nm and decreases by a factor of 1.4 and 118 for irradiations of 9.5 and 1.9 TW.cm^{-2} respectively (Fig. 5(c)).

Optical Materials EXPRESS

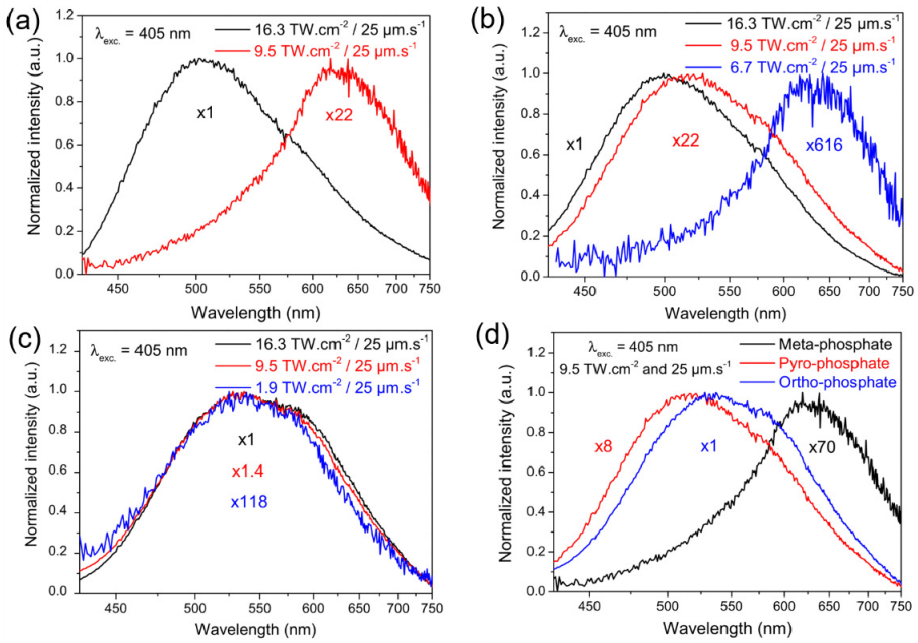

Fig. 5. Corrected spectral fluorescence emissions of photo-induced structures under laser diode excitation at 405 nm for three relevant compositions: (a) meta-phosphate GPN_{15}:Ag; (b) pyro-phosphate GPN_{26}:Ag; (c) ortho-phosphate GPN_{51}:Ag; (d) comparison of these three samples inscribed with 9.5TW.cm^{-2} at 25µm.s^{-1} (note that × 22 means that the absolute amplitude of the corresponding spectrum was multiplied by 22 to obtain the same normalized amplitude as that of the × 1 spectrum).

In order to highlight the distinct behavior of the three different phosphate glass network, their spectrum irradiated in the same conditions (9.5 TW.cm^{-2} and 25µm.s^{-1}) are superimposed in Fig. 5(d). The highest fluorescence intensity is obtained for the ortho-phosphate, followed by the pyro-phosphate glass (8 times lower), and the meta-phosphate (70 times lower).

4. Discussion

The progressive increase in sodium oxide content leads to a progressive modification of the glass network and associated structure, which affects in turn its physico-chemical properties, its spectroscopic properties and finally its sensitivity to femtosecond laser irradiation. The investigated Na_2O-P_2O_5-Ga_2O_3 system exhibits a lot of similarities with the Na_2O-P_2O_5-Al_2O_3 system previously reported by Brow [24].

Indeed, at low Na_2O content (15 Mol%), the major Raman band contributions are being assigned to symmetric P-O-P bond stretching vibrations between two Q^2, and to (PO_2^-) symmetric stretching vibrations in Q^2 entities. These observations suggest that the glass structure is dominated by long phosphate chains formed of Q^2 tetrahedron sharing one common corner. The structural units agree with a meta-phosphate glass, with a ratio O/P of 3.1 to 3.2 that remains below the typical boundary of 3.25 [24]. By analogy with alumino-phosphate glass, gallium ions in meta-phosphate glasses is expected to occupy octahedral sites bridging the phosphate chains [16]. For compositions close of meta-phosphate glasses in the $NaPO_3$-Ga_2O_3 system, Hee *et al.* and Eckert *et al*. demonstrated that gallium ion occupy in majority octahedral sites [17,34]. In the Raman spectroscopy, a GaO_6 vibration mode is attended to be peaked at 350 cm^{-1} [19] where the Raman assignments are tricky. A ^{71}Ga nuclear magnetic resonance study would help to better characterize the gallium octahedral site.

Optical Materials EXPRESS

Beyond this boundary, the glasses from 26 to 47 Mol% Na_2O content, correspond to a pyro-phosphate glass, with an O/P ratio ranging between 3.25 and 3.75. This range of compositions corresponds to the shrinkage of the long phosphate chains, observed with the reduction of Raman signal from Q^2 entities. The Gallium changes its environment from six-fold to four-fold coordination [19,34].

Correlatively, one observes an increase of the di-phosphate elements depicted with the presence of Q^1 entities. For the GPN_{51}:Ag glass (O/P = 3.8), isolated (PO_4^{3-}) elements are observed, which is in good agreements with an ortho-phosphate network.

One can clearly observe that the glass structure and composition have an impact on the silver environment. Indeed, the spectroscopy of the meta-phosphate glass composition is dominated by the spectroscopic properties of isolated Ag^+ ions (sites A), although silvers pairing (sites B) are also present, as correlatively seen from the UV-shifted absorption band-gap edge (Fig. 2(d)) and both from the excitation and emission spectra (Fig. 2(d)). For pyro-phosphates and ortho-phosphates, both A/B-type emission evolution and absorption spectrum red-shifting indicate that a silver segregation occurs at the vitreous network scale. The direct laser writing in silver-containing phosphate glasses and the creation of silver clusters using a 1030 nm femtosecond laser is driven by a four-photon absorption process [32]. In this framework, the absorption edge position and its nature in the UV range are of importance concerning the efficiency of laser energy deposition and subsequent material modification. The four-photon wavelength (i.e. 1030/4 = 257 nm) corresponds to the absorption band attributed to the B-type sites. One can observe a correlation between the presence of such sites and the rising of the photosensitivity to femtosecond laser exposure, which is maximum for the ortho-phosphate (x = 51) and minimum for meta-phosphate (x = 15). Indeed, for identical intermediate laser irradiation conditions, meta-phosphate and pyro-phosphate glasses typically show fluorescence emission intensity 8 times and 70 times lower than that of the ortho-phosphate glass, respectively (Fig. 5(d)).

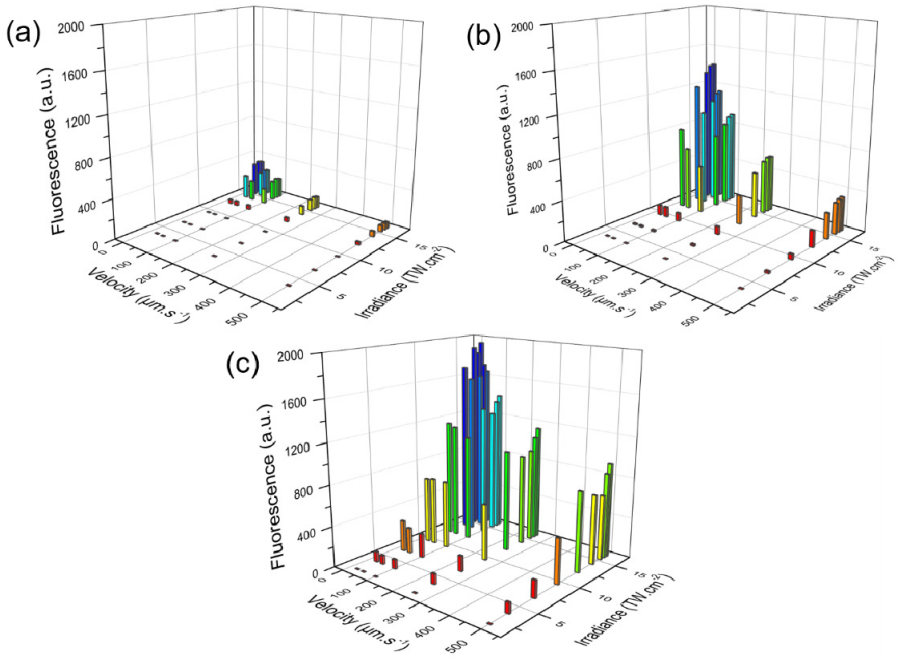

Fig. 6. Evolution of the integrated fluorescence imaging of all the photo-induced structures as a function of the velocity and irradiance for three typical glass compositions and associated structures (a) Meta-phosphate GPN_{15}:Ag (b) Pyro-phosphate GPN_{26}:Ag and (c) Ortho-phosphate GPN_{51}:Ag.

Optical Materials EXPRESS

To go further in the quantitative treatment of the three phosphate glass structures and their DLW photosensitivity, the "velocity-irradiance" matrix have been mapped. The luminescence intensity of all the produced structures have been integrated for the glasses GPN_{15}:Ag (Fig. 6(a)), GPN_{26}:Ag (Fig. 6(b)) and GPN_{51}:Ag (Fig. 6(c)). The laser-induced threshold for the formation of fluorescent silver clusters decreases from meta-, pyro- to ortho-phosphate glasses. This is accompanied with an increase of the fluorescence emission, similarly to what discussed in Fig. 5, as well as by an enlargement of the laser parameters range to achieve glass structuring.

The evolution of the integrated emission spectra of the three glasses with irradiance for a constant velocity of 25 $\mu m.s^{-1}$ is reported in Fig. 7. As shown in Fig. 6 for an excitation at 365 nm, it highlights the highest photosensitivity of the ortho-phosphate as compared to pyro- and meta-phosphate. Still, for hypothetical larger available laser irradiances, one cannot claim at this point whether the three different phosphate glasses would saturate to a similar fluorescence intensity level or if the ortho-phosphate would always lead to a larger fluorescence response. Moreover, the increase of laser irradiance will also reach optical damage threshold, which limits at some point the full consumption of silver element reservoir to grow fluorescent silver clusters. Thus, we believe that the ortho-phosphate glass is expected to keep being more photosensitive than the other compositions.

The emission spectra collected from the laser-written structure indicate a relation between the glass structure and the nature of the electron trap centers. At the lowest femtosecond laser irradiance, the laser-induced low fluorescence emission is observed in the red range with a maximum around 650 nm, which is attributed to Ag^{2+} for the meta- and pyro-phosphate compositions (Figs. 4(d), 4(e) and 5(a)). This traduces a weak laser-matter interaction associated with the formation of hole traps, with no clear evidence for the formation of silver clusters. This phenomenon is present for meta-phosphate up to 9.5 $TW.cm^{-2}$ irradiance while for pyro-phosphate it is noticeable only for 6.7 $TW.cm^{-2}$ irradiance. The nature of the silver ions environment, together with the silver mobility, play a strong role in terms of electron hole centers and/or electron donors (Ag^{+} + hole $\rightarrow$ Ag^{2+} and/or $Ag^{+} \rightarrow Ag^{2+} + e^{-}$), and of electron trap centers ($Ag^{+} + e^{-} \rightarrow Ag^{0}$) formation and stabilization. For such irradiation conditions, the glass matrix does not allow for a sufficient creation and/or mobility of Ag^{0} or Ag^{+} species. One can also suspect that the redox matrix potential poorly allows for the creation and stabilization of silver clusters. It remains that the electron hole centers formed on silver sites (Ag^{2+} and Ag^{0}) prevent the creation of phosphorous oxygen hole centers (such as PO_2^{2-}, POHC) supported by the phosphate network, as evidenced with the existence of a weak, red fluorescence emission attributed to Ag^{2+} species [32,35]. At higher femtosecond laser irradiance (16.3 $TW.cm^{-2}$), leading to a more efficient production of free electrons, such Ag^{2+} hole traps vanish, and silver cluster fluorescence appears. It suggests that the local glass matrix becomes more reductive, possibly accompanied with a chemical glass rearrangement including molecular oxygen release [36].

One can notice that for ortho-phosphates, no significant evidence of this red emission has ever been observed with these different conditions of irradiance. Even for very low laser irradiation (1.9 $TW.cm^{-2}$), fluorescence emission spectroscopy did not evidence the presence of Ag^{2+} hole traps, meaning that these species are not stabilized in such an ortho-phosphate glass. Correlatively, silver clusters are easily stabilized since they appear even for such very low irradiance, systematically leading to the same fluorescence spectral emission (Fig. 5(c)). This seems to be due to a better absorption capability of the laser irradiation (Fig. 2(d)) and a high initial quantity of Ag^{+}-Ag^{+} silver pairings (Fig. 3(b) and 3(c)) which allows for generating the smallest silver clusters (Ag^{+}-$Ag^{+} + e^{-} \rightarrow Ag_2^{+}$). Direct laser writing has been validated not only for constant molar percentage of silver but also on sample series having a constant silver concentration by considering the density of the glass. The silver mobility is also an important parameter since in the investigated glasses the Ag^{0} or Ag^{+} mobility is reported to increase thanks to the large amount of sodium ions [37,38]. The mobility of silver

Optical Materials EXPRESS

may also be affected by the modification of the role of sodium and silver ions, which are not only charge compensators for the gallium, especially in its tetrahedral coordination, but also can form Na-O ionic bonds.

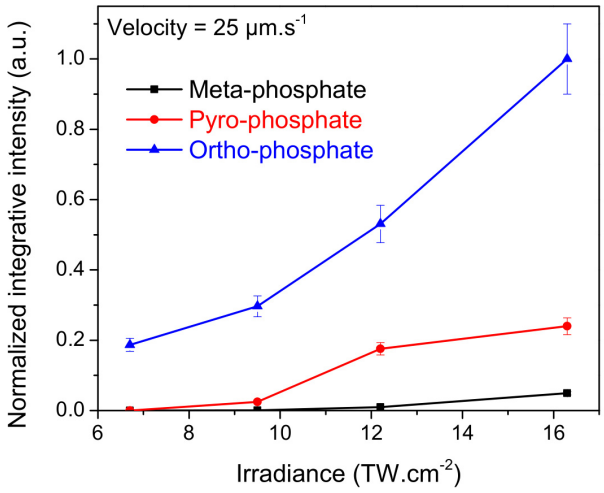

Fig. 7. Micro-fluorescence of the photo-induced structures and associated normalized spectrally-integrated intensity in a meta-, pyro- and ortho-phosphate glasses (GPN_{15}:Ag, GPN_{26}:Ag and GPN_{51}:Ag, respectively) versus irradiance for a 25 µm.s^{-1} sample velocity (excitation: 405 nm).

In summary, the variation in sensitivity to femtosecond laser irradiation discussed above may result from different aspects:

(i) the red-shifted position of the ortho-phosphate band-gap may allow for a better resonant four-photon energy deposition and electron release during the cumulative pulse-after-pulse irradiation, leading to a more efficient photo-activation of the silver-based chemistry, especially by increasing the amount of produced Ag^0 species that correspond to the first elementary precursors for the subsequent growth of larger silver clusters [39];

(ii) the presence of high sodium content and depolymerized phosphate chains may allow for a larger mobility of the precursors Ag^0 or Ag^+ in the growth of silver clusters;

(iii) the glass matrix redox properties may also show a more reductive behavior allowing for a more favorable stabilization of larger silver clusters (Fig. 5(c)).

Further work is needed to complete this study, including lifetime measurements of the produced species for the different glass compositions and the corresponding structure-property relationship. Additional work can also be considered to probe the correlative properties that appear concomitantly to the creation of silver clusters, including: (i) the nonlinear optical properties of third-harmonic generation (THG) [13] and the electric field-induced second harmonic generation (EFISHG) resulting from the stabilization of an embedded static and intense electric field [14]; (ii) the stability behavior under moderate thermal treatment (below 300°C [32,40]), for instance to dissociate traps (such as Ag^{2+}/Ag^0) and silver clusters.

5. Conclusion

We have investigated the influence of the sodium content in the P_2O_5 - Ga_2O_3 - Na_2O ternary system on the photosensitivity properties of the glass. Increasing the sodium content led to a drastic evolution of the glass network structure from a meta-phosphate made of long phosphate chains and inter-chains gallium ions to a pyro-phosphate containing phosphate

Optical Materials EXPRESS

dimmers and intra-chain gallium ions, to finally an ortho-phosphate network made of $[GaO_4]^-$ and $[PO_4]^{3-}$ units. Such shortening of the phosphate chains is accompanied by the progressive evolution of the silver environment from isolated ions Ag^+ to silver ions in close vicinity, such as Ag^+-Ag^+ pairs, exhibiting a red-shifted absorption as compared to isolated silver ions. This evolution offers a remarkable enhancement of the glass photosensitivity under femtosecond laser irradiation by lowering the laser structuring threshold for the creation of fluorescent molecular silver clusters. The reported work provides an extended approach to correlate structures and properties of sodium and silver containing photosensitive phosphate glasses. Such an investigation is highly relevant for applications where very bright 3D spatially-distributed fluorescent patterns are needed for the development, for instance, of fluorescent active waveguides, photonics integrated circuits or 3D high density optical data storage.

Funding

French Ministry of Education, the French National Research Agency (ANR) in the frame of the project ANR-17-CE08-0042-01, the "the investments for the future" Programme IdEx Bordeaux – LAPHIA (ANR-10-IDEX-03-02) and the Region "Nouvelle Aquitaine" in the frame of the FabMat project (2016-1R10107).

References

1. S. Gross and M. J. Withford, "Ultrafast-laser-inscribed 3D integrated photonics: challenges and emerging applications," Nanophotonics **4**(3), 332–352 (2015).
2. A. Podlipensky, A. Abdolvand, G. Seifert, and H. Graener, "Femtosecond laser assisted production of dichroitic 3D structures in composite glass containing Ag nanoparticles," Appl. Phys., A Mater. Sci. Process. **80**(8), 1647–1652 (2005).
3. Y. Dai, B. Zhu, J. Qiu, H. Ma, B. Lu, and B. Yu, "Space-selective precipitation of functional crystals in glass by using a high repetition rate femtosecond laser," Chem. Phys. Lett. **443**(4–6), 253–257 (2007).
4. Y. Shimotsuma, P. G. Kazansky, J. Qiu, and K. Hirao, "Self-organized nanogratings in glass irradiated by ultrashort light pulses," Phys. Rev. Lett. **91**(24), 247405 (2003).
5. Y. Bellouard, A. Said, M. Dugan, and P. Bado, "Fabrication of high-aspect ratio, micro-fluidic channels and tunnels using femtosecond laser pulses and chemical etching," Opt. Express **12**(10), 2120–2129 (2004).
6. K. Miura, J. Qiu, T. Mitsuyu, and K. Hirao, "Space-selective growth of frequency-conversion crystals in glasses with ultrashort infrared laser pulses," Opt. Lett. **25**(6), 408–410 (2000).
7. M. Vangheluwe, F. Liang, Y. Petit, P. Hée, Y. Ledemi, S. Thomas, E. Fargin, T. Cardinal, Y. Messaddeq, L. Canioni, and R. Vallée, "Enhancement of nanograting formation assisted by silver ions in a sodium gallophosphate glass," Opt. Lett. **39**(19), 5491–5494 (2014).
8. A. Royon, K. Bourhis, M. Bellec, G. Papon, B. Bousquet, Y. Deshayes, T. Cardinal, and L. Canioni, "Silver clusters embedded in glass as a perennial high capacity optical recording medium," Adv. Mater. **22**(46), 5282–5286 (2010).
9. S. D. Stookey, "Photosensitive glass," Ind. Eng. Chem. **41**(4), 856–861 (1949).
10. A. Abou Khalil, J.-P. Bérubé, S. Danto, J.-C. Desmoulin, T. Cardinal, Y. Petit, R. Vallée, and L. Canioni, "Direct laser writing of a new type of waveguides in silver containing glasses," Sci. Rep. **7**(1), 11124 (2017).
11. A. V. Podlipensky, V. Grebenev, G. Seifert, and H. Graener, "Ionization and photomodification of Ag nanoparticles in soda-lime glass by 150 fs laser irradiation: a luminescence study," J. Lumin. **109**(3-4), 135–142 (2004).
12. M. Bellec, A. Royon, K. Bourhis, J. Choi, B. Bousquet, M. Treguer, T. Cardinal, J.-J. Videau, M. Richardson, and L. Canioni, "3D Patterning at the Nanoscale of Fluorescent Emitters in Glass," J. Phys. Chem. C **114**(37), 15584–15588 (2010).
13. L. Canioni, M. Bellec, A. Royon, B. Bousquet, and T. Cardinal, "Three-dimensional optical data storage using third-harmonic generation in silver zinc phosphate glass," Opt. Lett. **33**(4), 360–362 (2008).
14. G. Papon, N. Marquestaut, Y. Petit, A. Royon, M. Dussauze, V. Rodriguez, T. Cardinal, and L. Canioni, "Femtosecond direct laser poling of sub-micron, stable and efficient second-order optical properties in a tailored silver phosphate glass," J. Appl. Phys. **115**, 113103 (2014).
15. N. Marquestaut, Y. Petit, A. Royon, P. Mounaix, T. Cardinal, and L. Canioni, "Three-Dimensional Silver Nanoparticle Formation Using Femtosecond Laser Irradiation in Phosphate Glasses: Analogy with Photography," Adv. Funct. Mater. **24**(37), 5824–5832 (2014).
16. R. K. Brow, "Brow, "Nature of Alumina in Phosphate Glass: I, Properties of Sodium Aluminophosphate Glass," J. Am. Ceram. Soc. **76**(4), 913–918 (1993).
17. P. Hee, R. Christensen, Y. Ledemi, J. E. C. Wren, M. Dussauze, T. Cardinal, E. Fargin, S. Kroeker, and Y. Messaddeq, "Properties and structural investigation of gallophosphate glasses by ^{71}Ga and ^{31}P nuclear magnetic

Optical Materials EXPRESS

resonance and vibrational spectroscopies," J. Mater. Chem. C Mater. Opt. Electron. Devices **2**(37), 7906–7917 (2014).
18. I. Belharouak, C. Parent, B. Tanguy, G. Le Flem, and M. Couzi, "Silver aggregates in photoluminescent phosphate glasses of the `Ag2O–ZnO–P2O5′ system," J. Non-Cryst. Solids **244**(2–3), 238–249 (1999).
19. A. Belkébir, J. Rocha, A. P. Esculcas, P. Berthet, B. Gilbert, Z. Gabelica, G. Llabres, F. Wijzen, and A. Rulmont, "Structural characterization of glassy phases in the system Na2O-Ga2O3-P2O5 by MAS and solution NMR and vibrational spectroscopy: II. Structure of the phosphate network," Spectrochim. Acta A Mol. Biomol. Spectrosc. **56**(3), 435–446 (2000).
20. J. Fukunaga, R. Bando, R. Ota, and N. Yoshida, "Raman Spectra and Structure of Glasses in the System Na2O-Ga2O3-B2O3," J. Ceram. Soc. Jpn. **96**(1114), 634–638 (1988).
21. A. Belkébir, J. Rocha, A. P. Esculcas, P. Berthet, S. Poisson, B. Gilbert, Z. Gabelica, G. Llabres, F. Wijzen, and A. Rulmont, "Structural characterization of glassy phases in the system Na2O-Ga2O3-P2O5 by MAS-NMR, EXAFS and vibrational spectroscopy. I. Cations coordination," Spectrochim. Acta A Mol. Biomol. Spectrosc. **56**(3), 423–434 (2000).
22. Y. Zhao and R. L. Frost, "Raman spectroscopy and characterisation of α-gallium oxyhydroxide and β-gallium oxide nanorods," J. Raman Spectrosc. **39**(10), 1494–1501 (2008).
23. D. Dohy and G. Lucazeau, "Raman Spectra and Valence Force Field of Single-Crystalline β Ga_2O_3," J. Solid State Chem. **45**(2), 180–192 (1982).
24. R. K. Brow, "Review: the structure of simple phosphate glasses," J. Non-Cryst. Solids **263–264**, 1–28 (2000).
25. D. Ilieva, B. Jivov, G. Bogachev, C. Petkov, I. Penkov, and Y. Dimitriev, "Infrared and Raman spectra of Ga2O3–P2O5 glasses," J. Non-Cryst. Solids **283**(1–3), 195–202 (2001).
26. L. L. Velli, C. P. E. Varsamis, E. I. Kamitsos, D. Möncke, and D. Ehrt, "Structural investigation of metaphosphate glasses," Phys. Chem. Glasses **46**(2), 4 (2005).
27. J. J. Hudgens, R. K. Brow, D. R. Tallant, and S. W. Martin, "Raman spectroscopy study of the structure of lithium and sodium ultraphosphate glasses," J. Non-Cryst. Solids **223**(1–2), 21–31 (1998).
28. B. G. Ershov, N. L. Sukhov, A. V. Kiseleva, and G. V. Ionova, "Silver clusters: Optical absorption and ESR spectra; structure and calculation of electron transitions," Russ. Chem. Bull. **45**(3), 545–549 (1996).
29. B. G. Ershov, G. V. Ionova, and A. A. Kiseleva, "Silver clusters: calculations of optical transitions and the formation and properties of "magic" positively charges clusters," Russ. J. Phys. Chem. **689**(2), 239–248 (1995).
30. I. Belharouak, C. Parent, P. Gravereau, J. P. Chaminade, G. Le Flem, and B. Moine, "Luminescent Properties of Silver(I) Diphosphate of Compositions $Na_{2-x}Ag_xZnP_2O_7$," J. Solid State Chem. **149**(2), 284–291 (2000).
31. J.-C. Desmoulin, Y. Petit, L. Canioni, M. Dussauze, M. Lahaye, H. M. Gonzalez, E. Brasselet, and T. Cardinal, "Femtosecond laser structuring of silver-containing glass: Silver redistribution, selective etching, and surface topology engineering," J. Appl. Phys. **118**(21), 213104 (2015).
32. K. Bourhis, A. Royon, M. Bellec, J. Choi, A. Fargues, M. Treguer, J.-J. Videau, D. Talaga, M. Richardson, T. Cardinal, and L. Canioni, "Femtosecond laser structuring and optical properties of a silver and zinc phosphate glass," J. Non-Cryst. Solids **356**(44–49), 2658–2665 (2010).
33. S. M. Hsu, S. W. Yung, R. K. Brow, W. L. Hsu, C. C. Lu, F. B. Wu, and S. H. Ching, "Effect of silver concentration on the silver-activated phosphate glass," Mater. Chem. Phys. **123**(1), 172–176 (2010).
34. J. Ren and H. Eckert, "Intermediate Role of Gallium in Oxidic Glasses: Solid State NMR Structural Studies of the Ga2O3–NaPO3 System," J. Phys. Chem. C **118**(28), 15386–15403 (2014).
35. K. Bourhis, A. Royon, G. Papon, M. Bellec, Y. Petit, L. Canioni, M. Dussauze, V. Rodriguez, L. Binet, D. Caurant, M. Treguer, J.-J. Videau, and T. Cardinal, "Formation and thermo-assisted stabilization of luminescent silver clusters in photosensitive glasses," Mater. Res. Bull. **48**(4), 1637–1644 (2013).
36. N. Varkentina, M. Dussauze, A. Royon, M. Ramme, Y. Petit, and L. Canioni, "High repetition rate femtosecond laser irradiation of fused silica studied by Raman spectroscopy," Opt. Mater. Express **6**(1), 79–90 (2016).
37. A. V. Dmitryuk, S. E. Paramzina, A. S. Perminov, N. D. Solov'eva, and N. T. Timofeev, "The influence of glass composition on the properties of silver-doped radiophotoluminescent phosphate glasses," J. Non-Cryst. Solids **202**(1–2), 173–177 (1996).
38. A. Pradel, T. Pagnier, and M. Ribes, "Effect of rapid quenching on electrical properties of lithium doncductive glasses," Solid State Ion. **17**(2), 147–154 (1985).
39. Y. Petit, K. Mishchik, N. Varkentina, N. Marquestaut, A. Royon, I. Manek-Hönninger, T. Cardinal, and L. Canioni, "Dual-color control and inhibition of direct laser writing in silver-containing phosphate glasses," Opt. Lett. **40**(17), 4134–4137 (2015).
40. A. Royon, K. Bourhis, L. Béchou, T. Cardinal, L. Canioni, and Y. Deshayes, "Durability study of a fluorescent optical memory in glass studied by luminescence spectroscopy," Microelectron. Reliab. **53**(9-11), 1514–1518 (2013).